



Click Chemistry

How to cite: Angew. Chem. Int. Ed. **2025**, 64, e202505585 doi.org/10.1002/anie.202505585

# **Imaging-Based High-Content Screening with Clickable Probes Identifies XPB Inhibitors**

Shuqi Li<sup>+</sup>, Hong-Rui Zhang<sup>+</sup>, Yang Yang, Ben Chi-Bun Ko, Jin Shang, Haijun Guo, Dan Yang, Mankin Wong, Ricky Wing-Cheung Chan, Karen Ka-Yan Kung, and Qian Zhao\*

Abstract: High-content screening (HCS) has become a powerful tool in drug discovery; however, its reliance on indirect readouts and surrogate markers limits HCS's ability to directly assess drug-protein interactions at endogenous levels, particularly in subcellular contexts. Here, we report an approach to address these limitations by combining confocal imaging-based HCS and bio-orthogonal labeling with clickable probes. As a proof-of-concept, we synthesized a probe Triptolide-alkyne (TL-alk) that rapidly and specifically labels xeroderma pigmentosum type B (XPB), a critical protein in nucleotide excision repair (NER). Probe-labeled XPB was conjugated to TAMRA to visualize the occupation of active sites, and EGFP and DAPI signals indicated XPB expression in the nucleus. Such a colorimetric HCS assay enabled the direct and precise measurement of drug occupancy rates in nuclear XPB of live cells. With this platform, pelitinib was identified as a novel ligand to bind XPB out of 1874 compounds containing. Food and Drug Administration (FDA)-approved drugs. Pelitinib formed a covalent bond with cysteine residue 342 of XPB, suppressed XPB's ATPase activity, impaired NER, and synergistically enhanced chemotherapy. This study not only overcomes limitations of HCS, but also demonstrates the transformative potential of bio-orthogonal labeling, such as in integration with HCS technologies, offering a novel framework for drug discovery targeting challenging protein systems.

#### Introduction

High-content screening (HCS) technologies combine automated imaging and sophisticated data analysis in a high-throughput format to quantitatively measure phenotypic changes in cells such as morphology,<sup>[1]</sup> viability,<sup>[2]</sup> proliferation,<sup>[3]</sup> and specific biomarker expression.<sup>[4]</sup> These measurements provide critical insights into the cellular effects of compounds, supporting lead optimization, toxicity assessment, and phenotypic screening.<sup>[5,6]</sup> Despite these strengths, traditional HCS platforms rely on indirect phenotypic readouts such as cell viability, morphology, or surrogate markers, which often fail to provide direct insights into drug-target interactions.<sup>[7]</sup> Overcoming these

challenges is crucial for a comprehensive understanding of drug activity, especially when dealing with complex or elusive protein targets.

Bio-orthogonal labeling enables the direct visualization of cellular activity of special protein targets through copper (I)-catalyzed azide-alkyne cycloaddition (CuAAC) click reaction with fluorescent reporters.<sup>[8]</sup> For example, to restore p53 activity by inhibiting the p53-MDM2 interaction, a set of probes based on 3-imidazolylindoles, a potent MDM2-p53 inhibitor class, containing different tags for bio-orthogonal chemistry were synthesized.<sup>[9,10]</sup> These probes could visualize the differential expression and the subcellular distribution of MDM2 and also determine the target occupancy of compounds. By conducting competition experiments between

[\*] S. Li<sup>+</sup>, Y. Yang, Dr. B. C.-B. Ko, J. Shang, H. Guo, R. W.-C. Chan, Dr. O. Zhao

Department of Applied Biology and Chemical Technology, The Hong Kong Polytechnic University, Hung Hom, Hong Kong SAR, P.R. China

E-mail: q.zhao@polyu.edu.hk

Prof. H.-R. Zhang+

College of Chemistry and Chemical Engineering and State Key Laboratory of Applied Organic Chemistry, Lanzhou University, Lanzhou 730000, P.R. China

Y. Yang

Centre for Eye and Vision Research, 17 W Hong Kong Science Park, Hong Kong, SAR 999077, P.R. China

Prof. D. Yang

Laboratory of Chemical Biology and Molecular Medicine, School of Life Sciences, Westlake University, Hangzhou 310024, P.R. China Dr. M. Wong, K. K.-Y. Kung

Department of Food Science and Nutrition, The Hong Kong Polytechnic University, Hung Hom, Hong Kong SAR, P.R. China

- [+] Both authors contributed equally to this work.
- Additional supporting information can be found online in the Supporting Information section
- © 2025 The Author(s). Angewandte Chemie International Edition published by Wiley-VCH GmbH. This is an open access article under the terms of the Creative Commons

Attribution-NonCommercial-NoDerivs License, which permits use and distribution in any medium, provided the original work is properly cited, the use is non-commercial and no modifications or adaptations are made.

36, Downloaded from https://onlinelibrary.wiley.com/doi/10.1002/anie.202505585 by HONG KONG POLYTECHNIC UNIVERSITY HU NG HOM, Wiley Online Library on [29/09/2025]. See the Terms and Conditions (https://onlinelibrary.wiley.com/terms

-and-conditions) on Wiley Online Library for rules of use; OA articles are governed by the applicable Creative Commons I

probes and tested molecules, ligands of specific proteins can be identified. [11,12] Although there are numerous good probes, they have been used to test only a handful of compounds because of the limited throughput of traditional gel-based or cell-based fluorescence imaging. When dealing with extensive compound libraries, new approaches are urgently needed to process multiple compounds in a single experiment.

We proposed a promising solution that combines bioorthogonal labeling with HCS, which could maximize their respective advantages. As a proof-of-concept, Xeroderma pigmentosum type B (XPB), the ATPase and a core subunit of the transcription factor TFIIH complex, was chosen as the drug target in our screening because of its critical role in nuclear excision repair (NER), and chemotherapy makes XPB an attractive therapeutic target.[13,14] Besides. the extremely low endogenous abundance and difficulties in expressing recombinant XPB in vitro challenge traditional biochemical assays. These factors collectively highlight the need for a novel HCS platform to study important proteins like XPB.<sup>[15]</sup> The lack of tools has impeded the development of XPB inhibitors, resulting in the identification of only one reported XPB covalent binder, Triptolide (TL), at the cysteine residue 342 (Cys342).[16,17] Therefore, there is a need to develop new XPB inhibitors for NER suppression and to overcome drug resistance.

In the present study, we synthesized a probe triptolidealkyne (TL-alk) that labels XPB in live cells swiftly and specifically. With optimized parameters, we established a confocal imaging-based HCS platform employing TL-alk to quantify drug occupancy in nuclear XPB. In total, 1874 FDA-approved drugs were screened, and pelitinib (Pel) was identified as a novel inhibitor to bind XPB. Pel was validated to suppress XPB's ATPase activity, impair the NER process, and subsequently enhance chemotherapy efficacy. The successful combination of bio-orthogonal labeling with HCS opens new avenues for broad applications of bio-orthogonal probes in drug discovery. Integrating the scalability of HCS with the specificity of bio-orthogonal chemistry creates a framework that not only overcomes the throughput limitations of gel-based or traditional imaging techniques but also provides unprecedented mechanistic insights into subcellular drug dynamics in HCS.

#### **Results and Discussion**

#### Design and Synthesis of Chemical Probes for Labeling XPB in Live Cells

Initially, we synthesized two chemical probes, TL-alk and triptolide-azide (TL-az), based on the structure of TL (Figures 1a and S1-3). We modified the parental compound TL on the side chain hydroxyl group based on prior knowledge of the structure-activity relationship to retain the biological activities.<sup>[16]</sup> Both probes retained the essential 12,13-epoxide functional group, which serves as an electrophilic center for covalent bonding with Cys342 of XPB.<sup>[14]</sup> Terminal alkyne and azide groups were incorporated for CuAAC click chemistry. The activity of probes was

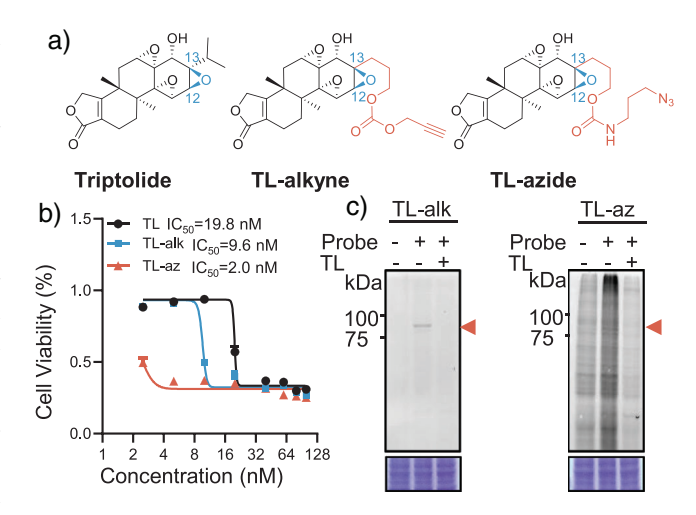


Figure 1. Structures and activities of TL and bio-orthogonal chemical probes. a) Structures of the TL, TL-alk probe, and TL-az probe. b) Cell viability of HeLa cells upon incubation with TL, TL-alk, or TL-az at different concentrations for 48 h. All data are presented as mean  $\pm$  SEM of three independent experiments. c) The in-gel fluorescence scan of proteins labeled with TL-alk and TL-az. HeLa cells were pre-treated with DMSO or TL, incubated with TL-alk or TL-az, and conjugated with TAMRA-azide or TAMRA-alkyne via CuAAC. Figure c contains cropped images of gels, and full uncropped versions are available in Supporting Information.

evaluated by measuring cell viability after treating HeLa cells for 48 h with various concentrations. The half-maximal inhibitory concentration (IC<sub>50</sub>) values of TL-alk and TL-az were 9.6 nM and 2.0 nM, respectively, slightly lower than TL (19.8 nM) (Figure 1b). Next, the probe labeling was visualized by using an in-gel fluorescent scan. TL was used to compete with probes and distinguish between specific and non-specific labeling. TL-alk displayed much less non-specific labeling than TL-az (Figure 1c). The increased background with TL-az was likely attributed to the excess amount of TAMRA-alkyne in the CuAAC reaction. It was reported that once activated, the TAMRA-alkyne could not only react with azide but also engage in secondary reactions with protein nucleophiles, such as the sulfhydryl groups in cysteine residues.<sup>[18,19]</sup> Interestingly, a prominent protein band at approximately 90 kDa was strongly and specifically labeled by TL-alk, which was likely to be endogenous XPB. Comparative analysis revealed that TL-alk outperformed its azide counterpart, TL-az, in in-gel fluorescence assays due to reduced background signals, underscoring its superior specificity and utility for HCS applications.

#### Labeling of XPB by Probe Triptolide-alkyne in Live Cells

Next, we evaluated the characteristics of TL-alk for labeling XPB in live cells in terms of efficiency, specificity, and labeling rate. A dose-dependent experiment determined the saturation concentration of TL-alk for XPB labeling with the half-maximal effective concentration (EC $_{50}$ ) value (0.0926  $\mu M$ ) (Figure 2a). The fluorescence intensity of the XPB band increased with probe concentration, reaching

1521373, 2025, 36, Downloaded from https://onlinelthray.wiley.com/doi/10.1002/anie.202505585 by HONG KONG POLYTECHNIC UNIVERSITY HU NG HOM, Wiley Online Library on [2909/2025]. See the Terms

and-conditions) on Wiley Online Library for rules of use; OA articles are governed by the applicable Creative Commons License

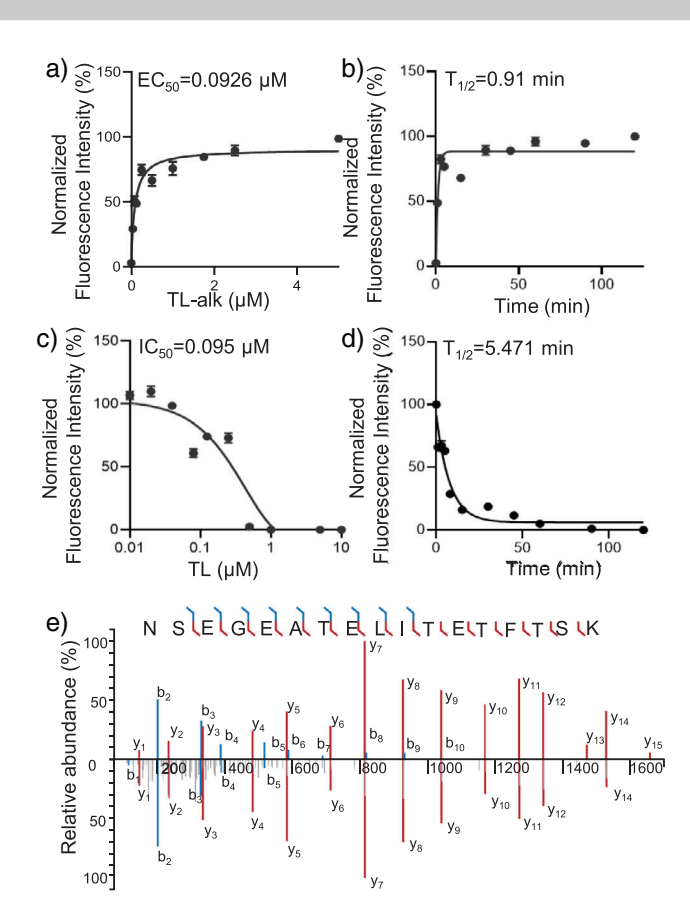


Figure 2. Validation of the robust and specific labeling of XPB with TL-alk. a) In a dose-dependent experiment, HeLa cells were treated with various concentrations (0, 0.04, 0.08, 0.125, 0.25, 0.5, 1, 1.75, 2.5, and  $5 \mu M$ ) of TL-alk for 30 min. b) In a time-course experiment, HeLa cells were treated with TL-alk for various periods (0, 1, 3, 5, 15, 30, 45, 60, 90, and 120 min). c) Dose-dependent TL competition labeling of XPB with the TL-alk probe in HeLa cells. HeLa cells were pre-treated with TL at various concentrations (0, 0.01, 0.02, 0.04, 0.08, 0.125, 0.25, 0.5, 1, 5, and 10  $\mu$ M) for 1 h, followed by treatment with 1  $\mu$ M TL-alk for 30 min. d) Time-course TL competition labeling of XPB with the TL-alk probe. HeLa cells were treated with DMSO or TL in various periods (0, 1, 3, 5, 15, 30, 45, 60, 90, and 120 min) for 1 h, followed by treatment with 1  $\mu$ M TL-alk for 30 min. The curves show the quantification of the fluorescence signal for each band, e) Mirrored theoretical (top) and experimental (bottom) mass spectra of the NSEGEATELITETFTSK peptide from XPB. The two spectra's similarity was measured by Spectral angle (SA = 0.49 > 0.3) and Pearson's correlation coefficient (PCC = 0.69 > 0.3).

saturation at  $0.25~\mu M$  without increasing non-specific labeling (Figure S4A). In a time-course experiment to investigate the labeling rate, the fluorescent intensity in the XPB band reached saturation within 3 minutes (Figures 2b and S4B). TL-alk showed high specificity, efficiency, and rapid labeling kinetics attributes that are critical for imaging-based assays designed to monitor dynamic processes in complex biological systems.

We also assessed TL's saturation concentration, finding that 1  $\mu$ M TL fully occupied endogenous XPB in HeLa cells (Figures 2c and S4C). TL reacted quickly: within 8 min, 10  $\mu$ M TL completely blocked TL-alk from labeling XPB (Figures 2d and S4D). To ensure consistency across different cell lines, we

tested the probe in HEK293T and HeLa S3 cells, achieving reproducible, specific, and rapid labeling (Figure S5).

Next, we employed TL-alk as a tool to visualize the subcellular localization of XPB. However, as a transcription factor,[14] endogenous XPB presents in extremely low abundance, making it difficult to observe under a regular confocal microscope. Therefore, we generated HEK293T and CHO-K1 cell lines that stably express EGFP-tagged XPB to visualize XPB more accurately, as the 121 kDa protein band in Figure S6A-C. To saturate tagged XPB in engineered cells, 5 µM of TL-alk was required (Figure S7B), and thus adopted in the following experiments. We designed a colorimetric assay with three channels to monitor EGFP, TAMRA, and DAPI stains. The EGFP signal was used to monitor the expression level and subcellular distribution of EGFP-tagged XPB. Through click chemistry, we conjugated TAMRA-azide to visualize probe-labeled XPB. The DAPI signal enabled cell counting and cytotoxicity assessment. Notably, while the IAA probe (negative control) exhibited a non-specific distribution, the TL-alk signals (the TAMRA signal) showed precise co-localization with EGFP-tagged XPB, confirming the probe's high specificity. Dose-response studies revealed an EC50 value of 0.604 µM, which aligned with independent in-gel fluorescence scan analysis (Figure S7D). The CHO-K1 XPB-EGFP cells are indeed a promising model for studying and visualizing the binding kinetics between XPB and TL-alk.

We also quantified the labeling efficiency of TL-alk with endogenous XPB by mass spectrometry (MS). Given its intrinsic low abundance, the basal level of XPB was undetectable in the control group. A strong signal of unique XPB peptide, "NSEGEATELITETFTSK", was observed after TL-alk enrichment (Figure 2e). These results demonstrated that TL-alk specifically and effectively labels XPB in live cells.

## The Cell Imaging-Based High-Content Screening (HCS) Assay with the Clickable Probe for Discovering XPB Inhibitors

Confocal fluorescence imaging showed that TL completely occupied XPB in CHO-K1-XPB-EGFP cells, as indicated by the lack of TAMRA signals (Figure S8A). This finding highlights the effectiveness of our approach and underscores the potential of direct intracellular imaging HCS assay as a reliable method for identifying XPB inhibitors (Figure 3a).

To ensure high reproducibility and robustness in cell-based HCS, we optimized the assay parameters to enhance signal differentiation between low and high readouts. TL was utilized as a benchmark to evaluate the binding effect, with 100 nM for low occupancy and 10 μM for strong competition with the probe for XPB binding. We compared fluorophores, blocking buffer, and washing buffer recipes to identify the most effective conditions (Figures 3b,c and S8B). The key factors for improving the signal window were the concentration of fluorophores and the use of a 0.5% casein-blocking buffer in the click reaction. Results (conditions a and b) showed that the saturation fluorophore concentration was required to achieve the highest TAMRA signal intensity. Also importantly, using the blocking buffer (conditions a and c) significantly reduced background noise

36, Downloaded from https://onlinelibrary.wiley.com/doi/10.1002/anie.202505585 by HONG KONG POLYTECHNIC UNIVERSITY HU NG HOM, Wiley Online Library on [29/09/2025]. See the Term

ditions) on Wiley Online Library for rules of use; OA articles are governed by the applicable Creative Commons L

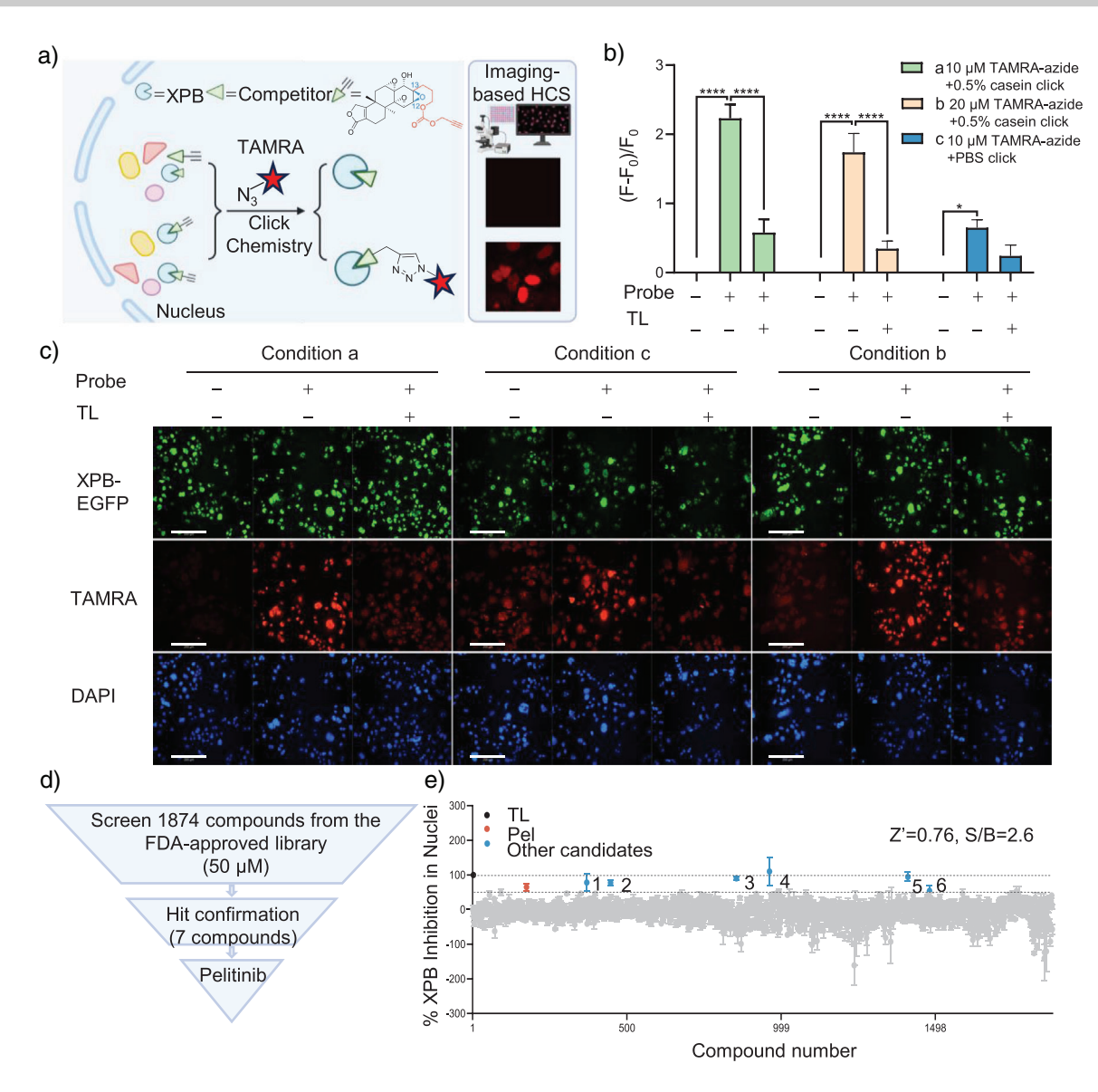


Figure 3. An imaging-based HCS was conducted to screen FDA-approved drugs for the identification of XPB-binding compounds. a) Schematic representation of the competition assay using TL-alk as a probe for visualization and illustrating the HCS workflow. b) Optimization of the cell imaging-based HCS assay. Condition a: 10 μM TAMRA-azide and click reaction in 0.5% casein-blocking buffer. Condition b: 20 μM TAMRA-azide and click reaction in 0.5% casein-blocking buffer. Condition c: 10 μM TAMRA-azide and click reaction in PBS. c) Representative fluorescence images for conditions a, b, and c. Scale bar =  $500 \mu$ M. d)Scheme for screening the FDA-approved library. A positive hit (pelitinib, Pel) was selected. e) The percentage of inhibition on labeling of XPB inside the nuclei. A threshold of > 50% XPB inhibition was used to identify positive candidates. Blue dots, high toxicity or unfavorable outcomes in validation. Black dot: TL as a positive control; Red dot: Pel; Blue dots: other tested compounds. All data are presented as mean  $\pm$  SEM of at least three independent experiments. Statistical analysis was performed using Two-way ANOVA with multiple comparisons; \*\*\*\*\*p < 0.0001, \*\*\*p < 0.001, and \*\*\*p < 0.001.

from unbound fluorophores. There was almost minimum difference between 0.1% Triton X-100 and 0.1% Tween-20 in removing excess fluorophores (Figure S9). The most effective combination in our assay was condition a, which successfully differentiated positive from negative results and was subsequently implemented in the subsequent HCS assay. The quantification and normalization of XPB labeling signals across groups were based on the formula: XPB labeling extent (F) = Mean Nucleic TAMRA (647) intensity / Mean Nucleic EGFP-tagged XPB intensity. The signal-to-noise ratio was determined via  $(F-F_0)$  /  $F_0$ , where  $F_0$  represents the

DMSO group result. To evaluate nuclear XPB competition and identify potential hit candidates, we applied the formula:  $((F_{probe}-F)/(F_{probe}-F_{TL}))$ .

A library of 1874 FDA-approved drugs was selected for XPB inhibitor screening due to their established safety profiles and repurposing potential. [20] Initial screening was performed, with compounds incubated at 50  $\mu$ M for 1 h, followed by a 0.5 h treatment with TL-alk. The short incubation period was used to identify compounds with fast-binding kinetics in XPB. The screening was conducted in triplicate, allowing for the exclusion of compounds







exhibiting high toxicity, which could confound the results. Candidate compounds were shortlisted if they yielded a 50% decrease in fluorescent intensity and did not cause any cell death, according to the DMSO-treated group. In Figure 3e, compounds were analyzed based on their XPB inhibition percentages, with grey dots indicating negative hits, which are compounds that showed less than 50% inhibition. Blue dots represented hits that were later excluded due to high toxicity or unfavorable outcomes in validation. Among these compounds, Pel (marked as a red dot) stood out for its combination of low toxicity and high efficiency in binding XPB, making it particularly noteworthy for further investigation. To evaluate the performance of HCS, we calculated the Z'-factor and signal-to-background ratio (S/B). The average Z'-factor was 0.76 and the average S/B was 2.6, which are both above the commonly accepted threshold for reliability.<sup>[21]</sup> The performance of the seven positive hits from HCS was manually checked (Figure S11). While all six candidates showed reduced TAMRA signals, the DAPI signal reflected their cytotoxicity to be 6 (100%) > 4 (98%) > 5 $(90\%) > 3 (70\%) > 2 (0\%) \approx 1 (0\%) \approx \text{Pel } (0\%) \text{ given the}$ same number of cells was initially seeded in each well. (1: Verteporfin, 2: Menadione, 3: Thimerosal, 4: Zinc Pyrithione, 5: Bardoxolone Methyl, and 6: Nonivamide)

#### Validation of the Novel XPB Inhibitor Pelitinib

Pel is an EGFR inhibitor currently in Phase II clinical trials for non-small cell lung cancer (NSCLC) and colorectal cancer,[22,23] emerged as a notable hit in our screening. To evaluate its inhibitory effect on XPB binding, alternative fluorescence imaging with a classical confocal microscope was performed to label XPB with Pel at varying concentrations. A dose-dependent reduction in TAMRA signal intensity, was observed with increasing Pel concentrations, confirming that Pel competed with TL-alk for binding to XPB. (Figure 4a,b). We also conducted the dose-dependent competition experiments with the other two compounds (1) Verteporfin (Ver) and (2) Menadione (Men) in CHO-K1-XPB-EGFP cells, and they displayed distinct inhibition effects and toxicity profiles. Both Ver and Men demonstrated dose-dependent competition to probe labeling of XPB (Figure \$12). However, Men caused significant nuclear morphological changes and exhibited high toxicity at tested concentrations (Figure S13), which was not observed for Pel or Ver.

Subsequently, the Cellular Thermal Shift Assay (CETSA) was employed to assess the direct interaction between Pel and XPB.<sup>[24]</sup> The findings revealed that pre-incubation with Pel increased XPB's thermal stability, indicating a direct interaction between Pel and XPB (Figure S14). To elucidate whether Pel forms a covalent complex with XPB and its binding sites, we performed LC-MS/MS of the XPB-Pel complex. As expected, the peptide <sup>335</sup>SGVIVLPCGAGK<sup>346</sup> displayed a mass increase of +467.15 240 Da at Cys342, which corresponds to the theoretical mass of a single Pel molecule (Figure 4c).

We investigated whether Pel could inhibit the ATPase activity of XPB using a fluorescence assay in a plate-reader format to monitor ATP turnover. This assay couples ATP hydrolysis to NADH oxidation via pyruvate kinase (PK) and lactate dehydrogenase (LDH),<sup>[25,26]</sup> as shown in Figure S15A. The reaction involves the conversion of phosphoenolpyruvate (PEP) to pyruvate by PK, followed by the reduction of pyruvate to lactate by LDH, with each molecule of ATP hydrolysis correlating to a decrease in NADH fluorescence. XPB's ATPase activity was significantly inhibited by TL and Pel, as evidenced by reduced linear fit slopes representing ATP hydrolysis rates (Figures 5a and S15B).

Given that XPB plays an essential role in nucleotide excision repair (NER), the effect of Pel on NER was tested through quantifying UV-induced DNA lesions, specifically the 6-4 pyrimidine-pyrimidone photoproducts (6-4PPs), using an anti-(6-4) PP antibody.[15,27,28] Following treatment with Pel, cells were exposed to UVC irradiation and postincubated in a drug-free medium for three hours (Figures 5b,c, and \$16). In DMSO-treated controls, HeLa cells showed 13% (6-4) PP lesions. In contrast, for HeLa cells treated with 30 µM Pel, 45% of (6-4) PP lesions remained after UVinduced nucleotide excision. These findings demonstrated that Pel significantly impaired NER and suppressed the removal of UV-induced DNA damage. We also tested the activity of Ver and Men in terms of NER inhibition. As we expected, Ver and Men both demonstrated inhibition effect, which was consistent with our observations in HCS, whereas Ver induced morphology change of cell nucleus of HeLa cells. (Figure \$17). Eventually, we chose Pel as the focus in subsequent assays.

Previous research has shown that inhibiting XPB and NER enhanced the sensitivity of cancer cells to platinum-based chemotherapeutic agents.[29-31] Therefore, we anticipated seeing synergistic anti-cancer effects of Pel and oxaliplatin. To eliminate the confounding effects of EGFR inhibition, we intentionally chose HepG2 cells, which lack EGFR expression, to test the Pel-related synergistic effect.[32] Considering that the IC<sub>50</sub> dose of pelitinib in HepG2 cells was 3.32 µM (Figure 5d), a sub-therapeutic concentration of 1 µM Pel was chosen for combination therapy with oxaliplatin. Two control groups with either 0.1% DMSO or 1 µM Pel were incorporated as reference. Pel significantly enhanced HepG2 cell sensitivity to oxaliplatin, with a 3-fold reduction in the IC<sub>50</sub> value, decreasing it to 2.3  $\mu$ M (Figures 5e and S18A). The synergistic effect was represented by the Coefficient of Drug Interaction (CDI), with CDI values below 1 indicating synergy.[33] Across all tested oxaliplatin concentrations, CDI values were consistently below 1, confirming a synergistic effect on cell death. The calculation method and results of CDI values were provided in Figure \$18B and Table \$1.

#### **Broader Applications in Drug Discovery**

This study establishes a broadly applicable framework for drug discovery against challenging protein targets under defined conditions. Notably, this approach enables the interrogation of protein targets previously inaccessible to conventional methodologies, including insoluble proteins in lysates, proteins mediating protein–protein interactions

36, Downloaded from https://onlinelibrary.wiley.com/doi/10.1002/anie.202505585 by HONG KONG POLYTECHNIC UNIVERSITY HU NG HOM, Wiley Online Library on [29/09/2025]. See the Term

and-conditions) on Wiley Online Library for rules of use; OA articles are governed by the applicable Creative Commons License

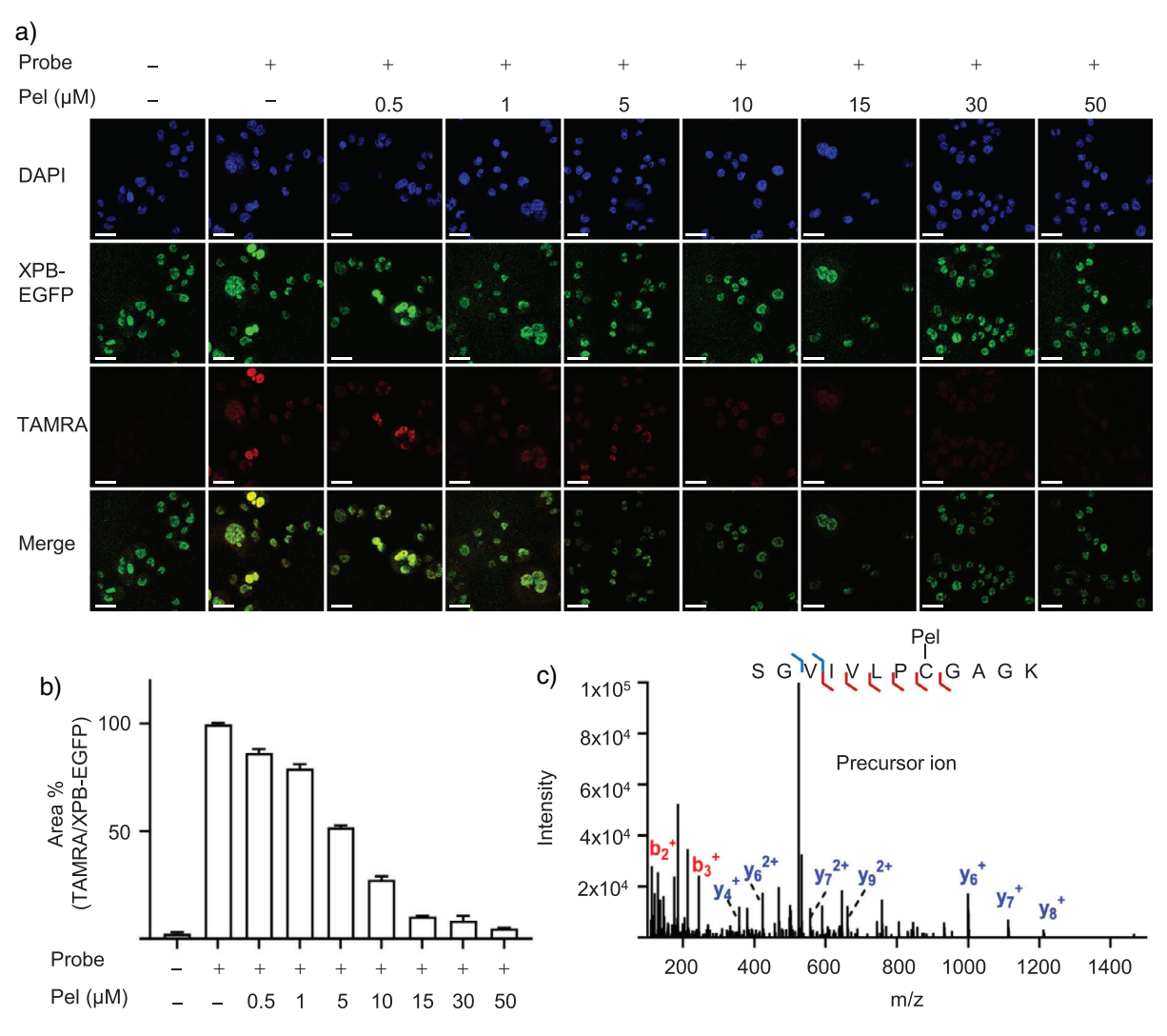


Figure 4. Validation of the interaction between Pel and XPB. a) A dose-dependent competition experiment showing probe-labeled XPB in the presence of Pel at indicated concentrations. Scale bar =  $25~\mu$ M. b) Quantification of fluorescence signals and area % of TAMRA/XPB-EGFP at different concentrations of Pel. c) LC-MS/MS analysis of Cys342-containing tryptic peptide after recombinant XPB was incubated with Pel 100  $\mu$ M. All data are presented as mean  $\pm$  SEM from at least three independent experiments.

(PPIs), and those requiring native conformations or physiological environments for ligand engagement. Furthermore, the platform facilitates high-throughput assessment of drug occupancy within specific organelles, cell types, or tissues. While we employed a cysteine-reactive probe bearing epoxide electrophiles, the strategy is readily adaptable to other bioorthogonal probes targeting lysine or alternative residues, provided sufficient selectivity is achieved. For example, this methodology could be extended to targets such as human murine double minute 2 (MDM2)<sup>[9]</sup> protein tyrosine phosphatase B (MptpB),<sup>[34]</sup> or G-Quadruplex(es) (G4).<sup>[35]</sup>

#### **Limitations and Future Directions**

Although chemical probes show varied specificities and kinetics in binding to their targets, not all chemical probes are suitable for establishing the HCS platform. Setting up an effective HCS platform will also require condition optimization and stable cell lines expressing tagged proteins, particularly for low-abundance targets such as XPB. After demonstrating the feasibility of combining bio-orthogonal labeling with the HCS platform, we will explore the possibility of using other chemical probes or additional biological systems. For example, extending our platform to primary cells, patient-derived models, or patient tissue slices could bridge the gap to clinical translation.

#### Conclusion

Our study presents a groundbreaking methodology for HCS that integrates bio-orthogonal probes with single-cell resolution imaging, enabling direct quantification of drug-target engagement in living systems. Through this imaging-based HCS platform, we screened 1874 FDA-approved drugs and



15213773, 2025,

36, Downloaded from https://onlinelibrary.wiley.com/doi/10.1002/anie.202505585 by HONG KONG POLYTECHNIC UNIVERSITY HU NG HOM, Wiley Online Library on [2909/2025]. See the Terms

ditions) on Wiley Online Library for rules of use; OA articles are governed by the applicable Creative Commons License

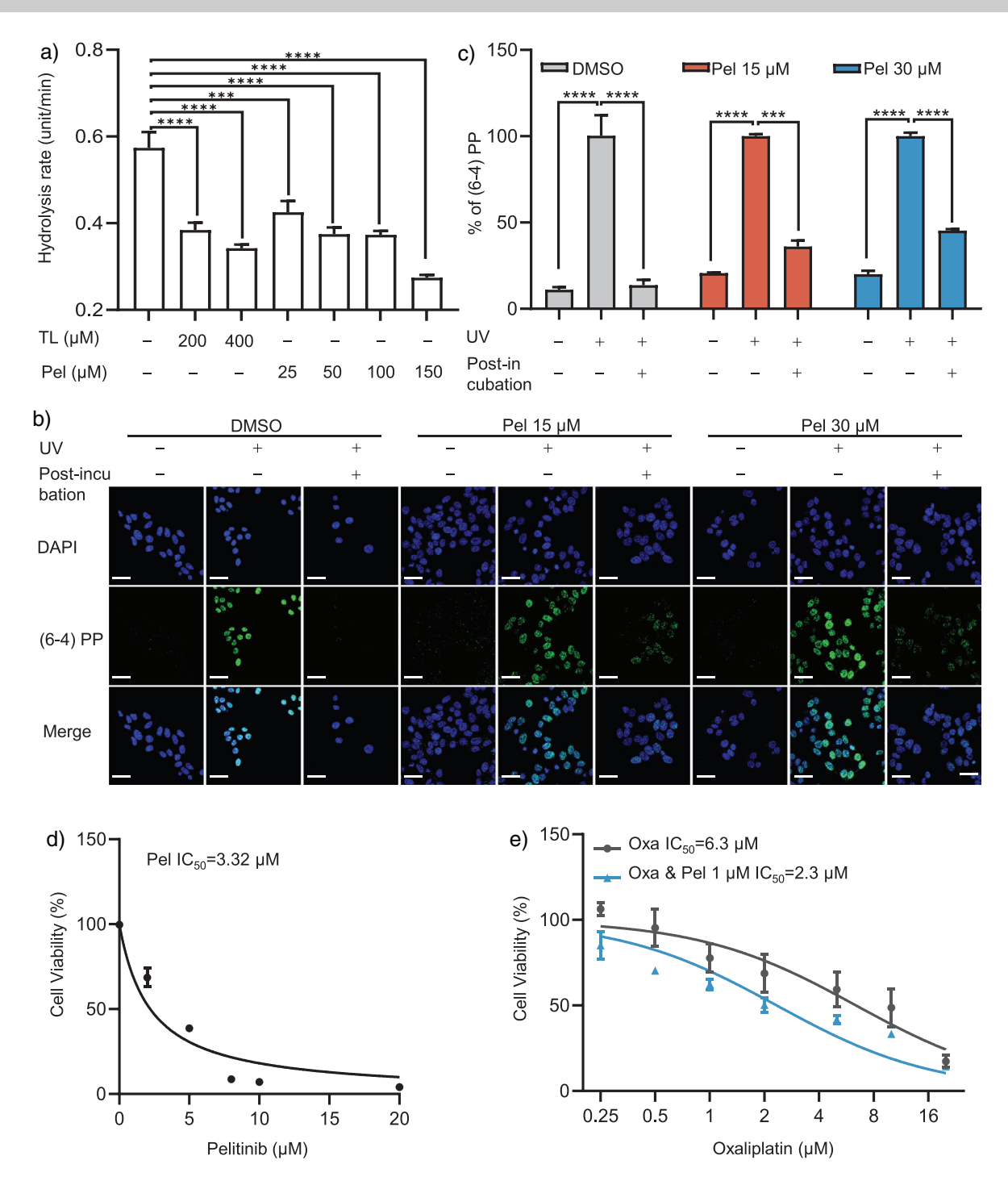


**Figure 5.** Pel inhibited the ATPase activity of XPB, suppressed NER, and synergized with oxaliplatin to kill cancer cells. a) ATPase activity of XPB in the presence of DMSO, TL, and Pel. b) Percentage of (6–4) PP lesions as an indicator of NER activity in the absence or presence of Pel. HeLa cells were exposed to DMSO or Pel for 1 h, irradiated with UVC (60 J m $^{-2}$ ), and post-incubated for 3 h in a drug-free medium. Subsequently, (6–4) PP lesions were labeled by using an anti-(6–4) PP antibody and detected by fluorescence microscopy. Scale bar = 25 μM. c) The y-axis represents the percentage of (6–4) PP lesions relative to the level measured immediately after irradiation for 0 h, which was set at 100% in all experiments. d) Cell viability of HepG2 cells upon incubation with different concentrations of Pel for 48 h. e) Evaluation of synergistic effects of Pel with oxaliplatin. Cell viability of HepG2 cells upon incubation with different concentrations of oxaliplatin (0.25–20 μM) in the presence of DMSO or Pel (1 μM) for 48 h. All data are presented as mean  $\pm$  SEM of at least three independent experiments. Statistical analysis was performed using Two-way ANOVA with multiple comparisons; \*\*\*\*p < 0.0001, \*\*\*p < 0.001, and \*\*p < 0.01.

15213773, 2025

36, Downloaded from https://onlinelibrary.wiley.com/doi/10.1002/anie.202505585 by HONG KONG POLYTECHNIC UNIVERSITY HU NG HOM, Wiley Online Library on [29/09/2025]. See the Terms

-and-conditions) on Wiley Online Library for rules of use; OA articles are governed by the applicable Creative Commons License

identified Pel as a novel XPB inhibitor. Mass spectrometry confirmed that Pel covalently binds to the Cys342 site of XPB. Functional studies demonstrated that Pel suppresses XPB's ATPase activity, impairs NER processes, and exhibits synergistic cytotoxicity with platinum-based chemotherapy agents in cancer cells. Compared to traditional XPB inhibitor TL, Pel offers reduced toxicity (IC<sub>50</sub> = 30 nM for TL<sup>[36]</sup> versus 3.32 µM for Pel in HepG2 cells). Critically, pel's established clinical trajectory—now in Phase II trials for NSCLC-contrasts with TL's stalled development due to safety concerns.[37,38] Furthermore, Pel's oral bioavailability and compatibility with combination therapies position it as a superior candidate for clinical applications. Although less potent than TL in inhibiting XPB, Pel's established clinical safety and reduced toxicity make it a promising candidate for drug repurposing. Although Pel showed potent XPB inhibition, its known EGFR-targeting activity may confound therapeutic applications. Future studies should evaluate isoform selectivity through CETSA profiling of EGFR versus XPB engagement. This HCS platform not only facilitated the identification of Pel as a promising XPB inhibitor but also underscored its potential to enhance cancer treatment through synergistic chemotherapy effects. Furthermore, the methodology establishes a robust framework for high-throughput drug discovery targeting complex protein systems, such as protein-protein interactions, thereby advancing precision medicine and addressing limitations of traditional HCS approaches that rely on indirect phenotypic readouts. The integration of HCS and bio-orthogonal labeling is not merely an alternative but a necessary evolution for difficult targets, where traditional tools are insufficient and recombinant proteins are unattainable. Our platform's ability to assess drug binding occupancy, kinetics, and subcellular specificity provides a level of precision critical for identifying novel inhibitors and understanding their mechanisms.

#### **Supporting Information**

The authors have cited additional references within the Supporting Information.[39–42]

#### **Acknowledgements**

The authors acknowledge the funding support provided by the Research Grants Council- GRF 15304819, GRF 15305821, Collaborative Research Fund (CRF) C5033-19E, and Research Imapet Fund (RIF) R5050-18. The authors also acknowledge the support from the Laboratory for Synthetic Chemistry and Chemical Biology Limited (LSCCB) and the Centre for Eye and Vision Research (CEVR) under the Health@InnoHK Programme launched by ITC, HKSAR. The authors thank the PolyU Research Facilities UCEA, ULS, RCSV, RiFood, and RCMI for technical support.

#### **Conflict of Interests**

The authors declare no conflict of interest.

#### **Data Availability Statement**

The data that support the findings of this study have been deposited to the ProteomeXchange Consortium (http://proteomecentral.proteomexchange.org) PRIDE partner repository with the dataset identifier PXD059271. Username: reviewer pxd059271@ebi.ac.uk; Password: OvgcZwVCFvcr.

**Keywords:** Click chemistry probes • High-content screening • Xeroderma pigmentosum type B

- [1] D. W. Young, A. Bender, J. Hoyt, E. McWhinnie, G.-W. Chirn, C. Y. Tao, J. A. Tallarico, M. Labow, J. L. Jenkins, T. J. Mitchison, Y. Feng, Nat. Chem. Biol. 2008, 4, 59-68.
- [2] M. Boutros, A. A. Kiger, S. Armknecht, K. Kerr, M. Hild, B. Koch, S. A. Haas, R. Paro, N. Perrimon, Science 2004, 303, 832-
- [3] E. Jan, S. J. Byrne, M. Cuddihy, A. M. Davies, Y. Volkov, Y. K. Gun'ko, N. A. Kotov, ACS Nano 2008, 2, 928-938.
- [4] P. Lang, K. Yeow, A. Nichols, A. Scheer, Nat. Rev. Drug Discovery 2006, 5, 343-356.
- [5] G. Nierode, P. S. Kwon, J. S. Dordick, S. J. Kwon, J. Microbiol. Biotechnol. 2016, 26, 213-225.
- [6] M. Boutros, F. Heigwer, C. Laufer, Cell 2015, 163, 1314-1325.
- [7] V. Kumar, P. K. Chunchagatta Lakshman, T. K. Prasad, K. Manjunath, S. Bairy, A. S. Vasu, B. Ganavi, S. Jasti, N. Kamariah, Heliyon 2024, 10, e23864.
- [8] C. Guo, Y. Chang, X. Wang, C. Zhang, P. Hao, K. Ding, Z. Li, Chem. Commun. 2019, 55, 834-837.
- P. L. D'Alessandro, N. Buschmann, M. Kaufmann, P. Furet, F. Baysang, R. Brunner, A. Marzinzik, T. Vorherr, T. M. Stachyra, J. Ottl, D. E. Lizos, A. Cobos-Correa, Angew. Chem. Int. Ed. Engl. 55, 16026-16030.
- [10] P. Furet, P. Chène, A. De Pover, T. S. Valat, J. H. Lisztwan, J. Kallen, K. Masuya, Bioorg. Med. Chem. Lett. 2012, 22, 3498-
- [11] N. M. Meghani, H. H. Amin, B. J. Lee, Drug Disco. Today 2017, 22, 1604-1619.
- [12] X. Wang, B. Huang, X. Liu, P. Zhan, Drug Disco. Today 2016, *21*, 118–132.
- [13] J. Luo, P. Cimermancic, S. Viswanath, C. C. Ebmeier, B. Kim, M. Dehecq, V. Raman, C. H. Greenberg, R. Pellarin, A. Sali, D. J. Taatjes, S. Hahn, J. Ranish, Mol. Cell 2015, 59, 794-806.
- [14] D. V. Titov, B. Gilman, Q. L. He, S. Bhat, W. K. Low, Y. Dang, M. Smeaton, A. L. Demain, P. S. Miller, J. F. Kugel, J. A. Goodrich, J. O. Liu, Nat. Chem. Biol. 2011, 7, 182-188.
- [15] A. M. Di Francesco, A. Ruggiero, R. Riccardi, Cell. Mol. Life Sci. 2002, 59, 1914–1927.
- [16] Q. L. He, D. V. Titov, J. Li, M. Tan, Z. Ye, Y. Zhao, D. Romo, J. O. Liu, Angew. Chem. Int. Ed. Engl. 2015, 54, 1859-1863.
- [17] J. Kohl, J. Ng, S. Cachero, E. Ciabatti, M. J. Dolan, B. Sutcliffe, A. Tozer, S. Ruehle, D. Krueger, S. Frechter, T. Branco, M. Tripodi, G. S. Jefferis, Proc. Natl. Acad. Sci. USA 2014, 111, E3805-E3814.
- [18] C. G. Parker, M. R. Pratt, Cell 2020, 180, 605-632.
- [19] A. E. Speers, B. F. Cravatt, Chem. Biol. 2004, 11, 535-546.
- [20] R. Huang, N. Southall, Y. Wang, A. Yasgar, P. Shinn, A. Jadhav, D. T. Nguyen, C. P. Austin, Sci. Transl. Med. 2011, 3, 80ps16-
- [21] J. Inglese, R. L. Johnson, A. Simeonov, M. Xia, W. Zheng, C. P. Austin, D. S. Auld, Nat. Chem. Biol. 2007, 3, 466-479.
- [22] A. Wissner, E. Overbeek, M. F. Reich, M. B. Floyd, B. D. Johnson, N. Mamuya, E. C. Rosfjord, C. Discafani, R. Davis,





15213773, 2025

36, Downloaded from https://onlinelibrary.wiley.com/doi/10.1002/anie.202505585 by HONG KONG POLYTECHNIC UNIVERSITY HU NG HOM, Wiley Online Library

on [29/09/2025]. See the Term

are governed by the applicable Creative Commons

- X. Shi, S. K. Rabindran, B. C. Gruber, F. Ye, W. A. Hallett, R. Nilakantan, R. Shen, Y.-F. Wang, L. M. Greenberger, H.-R. Tsou, *J. Med. Chem.* **2003**, *46*, 49–63.
- [23] R. Roskoski, Pharmacolo. Res. 2019, 139, 395-411.
- [24] R. Jafari, H. Almqvist, H. Axelsson, M. Ignatushchenko, T. Lundbäck, P. Nordlund, D. M. Molina, Nat. Protoc. 2014, 9, 2100–2122.
- [25] E. J. Tomko, O. Luyties, J. K. Rimel, C.-L. Tsai, J. O. Fuss, J. Fishburn, S. Hahn, S. E. Tsutakawa, D. J. Taatjes, E. A. Galburt, J. Mol. Biol. 2021, 433, 166813.
- [26] J. Luo, M. Kong, L. Liu, S. Samanta, B. Van Houten, A. Deiters, ChemBioChem 2017, 18, 466–469.
- [27] J. A. Marteijn, H. Lans, W. Vermeulen, J. H. J. Hoeijmakers, *Nat. Rev. Mol. Cell Biol.* 2014, 15, 465–481.
- [28] S. Alekseev, M. Ayadi, L. Brino, J. M. Egly, A. K. Larsen, F. Coin, Chem. Biol. 2014, 21, 398–407.
- [29] R. Szalat, M. K. Samur, M. Fulciniti, M. Lopez, P. Nanjappa, A. Cleynen, K. Wen, S. Kumar, T. Perini, A. S. Calkins, E. Reznichenko, D. Chauhan, Y. T. Tai, M. A. Shammas, K. C. Anderson, J. P. Fermand, B. Arnulf, H. Avet-Loiseau, J. B. Lazaro, N. C. Munshi, *Leukemia* 2018, 32, 111– 119.
- [30] S. Alekseev, M. Ayadi, L. Brino, J.-M. Egly, A. K. Larsen, F. Coin, Chem. Biol. 2014, 21, 398–407.
- [31] M. Ueda, K. Matsuura, H. Kawai, M. Wakasugi, T. Matsunaga, Genes Cells 2019, 24, 284–296.
- [32] C. Tian, R. Sun, K. Liu, L. Fu, X. Liu, W. Zhou, Y. Yang, J. Yang, Cell Chem. Biol. 2017, 24, 1416–1427.e5.

- [33] S. K. Sagwal, G. Pasqual-Melo, Y. Bodnar, R. K. Gandhirajan, S. Bekeschus, *Cell Death Dis.* **2018**, *9*, 1179.
- [34] L. P. Tan, H. Wu, P. Y. Yang, K. A. Kalesh, X. Zhang, M. Hu, R. Srinivasan, S. Q. Yao, Org. Lett. 2009, 11, 5102– 5105.
- [35] J. Lefebvre, C. Guetta, F. Poyer, F. Mahuteau-Betzer, M. P. Teulade-Fichou, Angew. Chem. Int. Ed. Engl. 2017, 56, 11365–11369.
- [36] D. Kang, Y. Liu, Y. Song, B. Fang, Q. Zhang, L. Hu, Front Oncol. 2022, 12, 811850.
- [37] X.-J. Li, Z.-Z. Jiang, L.-y. Zhang, J. Ethnopharmacol. 2014, 155, 67–79.
- [38] X. Lu, L. Yu, Z. Zhang, X. Ren, J. B. Smaill, K. Ding, Med. Res. Rev. 2018, 38, 1550–1581.
- [39] H. Xu, H. Tang, H. Feng, Y. Li, J. Org. Chem. 2014, 79, 10110– 10122.
- [40] D. Yang, Q. Gao, J.-J. Xue, Z. Deng, O. Y. Lee, Versitech Limited Morningside Ventures Limited, 2016.
- [41] O. Longin, H. van de Langemheen, R. M. J. Liskamp, *Bioorg. Med. Chem.* 2017, 25, 5008–5015.
- [42] W. G. Lewis, F. G. Magallon, V. V. Fokin, M. G. Finn, J. Am. Chem. Soc. 2004, 126, 9152–9153.

Manuscript received: March 10, 2025 Revised manuscript received: June 27, 2025 Accepted manuscript online: June 27, 2025 Version of record online: July 30, 2025